MID-INFRARED SPECTROSCOPY OF PERSISTENT LEONID TRAINS

RAY W. RUSSELL, GEORGE S. ROSSANO,
MARK A. CHATELAIN, DAVID K. LYNCH,
TED K. TESSENSOHN, ERIC ABENDROTH, AND DARYL KIM
Space Science Applications Laboratory,
The Aerospace Corporation, M2-266, P.O. Box 92957, Los Angeles, CA 90009-2957
E-mail: Ray.W.Russell@aero.org

and

PETER JENNISKENS
SETI Institute, NASA ARC, Mail Stop 239-4, Moffett Field, CA 94035

(Received 16 August 2000; Accepted 1 September 2000)

Abstract. The first infrared spectroscopy in the 3–13 micron region has been obtained of several persistent Leonid meteor trains with two different instrument types, one at a desert ground-based site and the other on-board a high-flying aircraft. The spectra exhibit common structures assigned to enhanced emissions of warm CH_4, CO_2, CO and H_2O, which may originate from heated trace air compounds or materials created in the wake of the meteor. This is the first time that any of these molecules has been observed in the spectra of persistent trains. Hence, the mid-IR observations offer a new perspective on the physical processes that occur in the path of the meteor at some time after the meteor itself has passed by. Continuum emission is observed also, but its origin has not yet been established. No 10 micron dust emission feature has been observed.

Keywords: Meteors, meteoroids, mid-IR spectroscopy, persistent trains

1. Introduction

Spectroscopy of meteors and persistent trains in the infrared (IR) part of the spectrum from about 3 to 13 microns has long been expected to be a useful tool in our efforts at understanding the composition of meteoroids

and how they interact with the Earth's atmosphere (Jenniskens and Butow, 1999).

Shower meteoroids originate in the dust grains thrown off from parent comets, 55P/Tempel-Tuttle in the case of the Leonids, and follow similar orbital paths for long periods of time. Our group at The Aerospace Corporation has been studying the thermal spectra of comets for many years (e.g., Hanner *et al.*, 1994) in order to determine the temperature, composition, and morphology of cometary dust grains. In the case of comet 55P/Tempel-Tuttle, the thermal IR emission of dust in the comet coma showed a gray body behavior that is typical of large grains or organic materials (Lynch *et al.*, 2000), but not very diagnostic of the detailed nature of the grains.

During the heating of the grains as they interact with the atmosphere as meteors, meteoroid fragments, molecules, or even atoms are separated from the grain in a process of ablation (Boyd, 2000; Popova, 2000), and are heated sufficiently to exhibit spectral signatures that could shed additional light on at least the underlying composition of these grains. The thermal emission from the heated grains striking the atmosphere will appear first in the long wave IR, and shift to shorter wavelengths as the body gets hotter. The meteor's kinetic energy is sufficiently large to completely vaporize the meteoroid.

Moreover, the kinetic energy is sufficiently large to heat a significant volume of air in the mesosphere and lower thermosphere. Long persisting luminous glows are seen at visual wavelengths in the path of bright Leonid fireballs, called "persistent trains," which allow pointing at and tracking of this heated air.

The first published mid-IR broadband detections of meteors, but no spectra, were obtained during the 1998 Leonid Multi-instrument Aircraft Campaign (Jenniskens and Butow, 1999) and are presented in Rossano, *et al.* (2000). The problem with attempts at IR spectroscopy of transient phenomena such as meteors has been the difficulty in capturing the signals themselves with IR sensors with sufficient sensitivity, a large enough spatial field of view and yet fine enough spatial resolution, and spectral resolution to permit the analysis of these phenomena. Major advances in recent years in IR sensor design, detector arrays, and data acquisition systems have created the capability to acquire, track, and measure these phenomena with sufficient sensitivity to provide meaningful datasets with which to investigate meteor-related phenomena.

This paper reports the first mid-IR spectra of Leonid persistent trains obtained with an imaging spectrograph, taking full spectra with each scan, situated onboard the 1999 Leonid Multi-instrument Airborne Campaign (Leonid MAC) on a mission to the Mediterranean, and with a wavelength-scanning spectrometer on the ground at the Starfire Optical Range at Kirtland AFB in New Mexico.

2. The Observations

The data were acquired with the Aerospace Mid-wave InfraRed Imaging Spectrograph (MIRIS) and the Circular Variable Filter wheel spectrometer (CVF). The MIRIS uses a liquid nitrogen-cooled 2D 256 x 256 InSb array and a grism (combination grating and prism, Rossano *et al.* 2000) to obtain long-slit spectra and zeroth order broadband images in the 3-5.5 micron spectral region (ibid). The slit was constructed to permit slitless spectroscopy and imaging of meteors in the center 128 rows of the array, and also to permit narrow slit (5 pixels wide in the dispersion direction) spectroscopy of meteor persistent trains in the 64 rows near the top of the array and the 64 rows near the bottom of the array. MIRIS was deployed aboard the USAF Flying Infrared Signature Technology Aircraft (FISTA) as part of the 1999 Leonid MAC effort (Jenniskens *et al.*, 2000). The spectral resolving power is about 50 (due to the extended nature of the source and the slit width), and spatial pixel size was about 0.8 mrad (0.046 ^{o}). The sensor viewed the sky through a ZnSe window while the FISTA was flying at about 10–12 km, where the sensor was above the majority of the Earth's atmosphere and more than 99% of the water vapor. Complete spectra were obtained at 24 frames per second with an observing efficiency of about 40%, generating gigabytes of data during the MAC.

The CVF uses three multi-layer interference wedges and an Si:As back-illuminated blocked impurity band (BIBIB) detector element cooled to liquid helium temperatures to obtain spectroscopy from 2.5 to 14.5 microns with a spectral resolving power of about 60, with an off-axis parabola as the collecting optic in a custom setup created for this event. It was mounted on a steerable alt-azimuth telescope mount at the Starfire Optical Range (SOR), Kirtland AFB (New Mexico), and the field of view was approximately 0.25 degree. Data were obtained in a step-and-integrate mode as DC voltages with the sensor viewing the sky or sky plus meteoroid train. Each spectrum required about 5–10 minutes

to acquire. Spectra on the meteor trains were compared to spectra of the sky at the same elevation angle but at a slightly different (delta of about 15°) azimuth. Sky spectra were very consistent over the course of the night, facilitating the accurate subtraction of atmospheric and sensor emissions contributing to the spectral signals measured while observing the persistent meteor trains.

The wavelength calibration of the MIRIS was achieved through the use of known absorption features in calibrated pieces of plastic and was good to about 0.03 microns. The plastic materials, none of which was a commercial calibration product, were taken from a variety of sources and their absorption wavelengths calibrated on a Fourier Transform spectrometer. The CVF wavelength calibration was performed with an Oriel single-pass grating monochromator to better than 0.3 of a spectral resolution element, where a spectral resolution element is about 0.017 times the wavelength. The radiometric calibrations of both sensors were accomplished through observations of extended blackbodies designed and built for this purpose at The Aerospace Corporation. These sources have been compared to NIST-traceable cavity blackbodies and shown to have an emissivity of about 95–98% over the entire spectral range of interest here except in the 8–10 micron region, where a small (~10%) dip is observed due to glass beads in the 3M Black Velvet paint used to coat the blackbodies. The blackbodies are heated by Kapton-coated extended heater elements and controlled through either an automatic servo-controlled heater or by manual control of a Variac transformer, in both instances using thermocouples on the blackbodies to determine the temperature of the sources. There is an absolute temperature uncertainty in the surfaces of the blackbodies of about 1–2 K due to the uncertainty from the thermocouple and the paint thickness and non-uniformities over the surface of the blackbodies. The temperature stability was typically 0.2 K.

Both IR sensors utilized bore-sighted optical sensors (CCDs) to obtain starfield information for pointing determination and for direct simultaneous viewing of the meteor trains that were being measured in the IR. Pointing alignment between the IR and visible scenes was verified using bright sources such as the moon and man-made sources (landing strip lights). At SOR, initial visual sightings of the trains led to verbal direction to steer the sensors toward a particular part of the sky, and then visible CCD images were used to guide the commanding of the telescope mount to perform fine positioning of the IR beam onto the train. For the FISTA observations, initial detections in the visible caused

a command to turn the plane to a proper heading, and then the eyeball mount was steered by hand while monitoring the CCD image to position the slit of the IR sensor on the train.

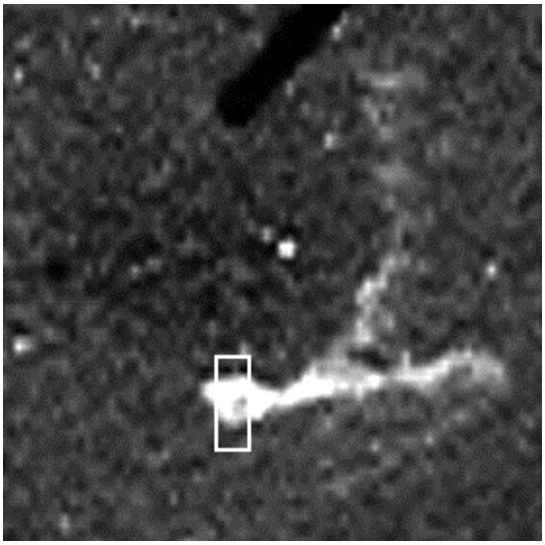

Figure 1. Approximate position of the MIRIS slit on the "Y2K" persistent train at 04:02:19 UT on Nov. 18, 1999. The white box indicates the location of the MIRIS slit and the dark marker in the top center of the image was used for positioning the camcorder relative to the image intensifier.

3. Results

3.1. MIRIS RESULTS

The airborne MIRIS data were obtained the night of the storm, 18 Nov. 1999 UT, with the best spectrum recorded being that of the so-called "Y2K" train (Figure 1), caused by a –13 magnitude Leonid fireball at 04:00:29 UT (Jenniskens and Rairden, 2000). The train was observed from about 04:02 to 04:09 UT. During our observations, the train was at an altitude of 83.2 ± 1.0 km, which corresponds to positions 14–18 in Jenniskens and Rairden (2000), at a distance of 205 km from the FISTA aircraft and 19^{o} above the eastern horizon at the airplane's altitude.

The train was observed by MIRIS in both zeroth and first orders. It was first observed as a zero order image in the slitless region of the

spectrograph, and then MIRIS was repositioned to place the brightest part of the train onto the narrow slit which spanned the upper 64 rows of the array. The train spectrum was observed over approximately 8 rows up and down the narrow slit. Adjacent rows on the array do not show the enhanced signal levels seen on the train and were used to subtract the signals due to sky emission and instrumental background from the train spectra. An average scan was made of about 20 frames, representing 10 msec exposure each at 1m50s after the fireball, at a time when the brightest part of the train was first positioned in the slit of the spectrograph (Figure 1).

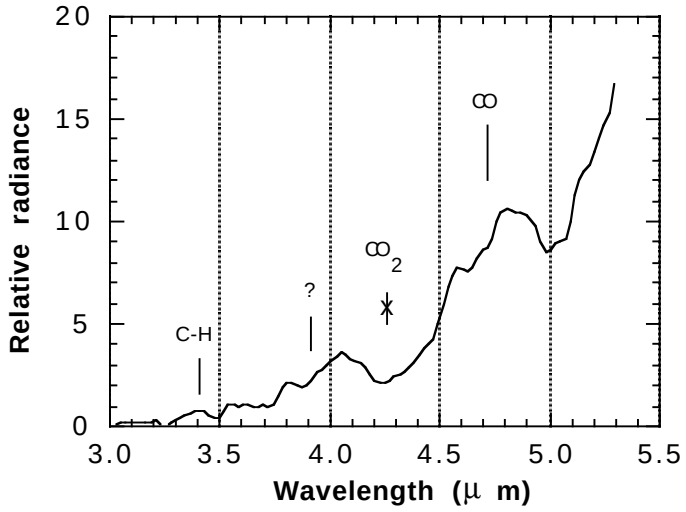

Figure 2a. Linear plot of the intensity from the "Y2K" train at 04:02:19 UT reported by MIRIS.

Figure 2a shows the MIRIS data on a linear plot. Superposed on a continuum that rises towards longer wavelengths are seen several broad emission features. A small feature at 3.4 micron is readily identified as the C-H stretch vibration band, possibly of the molecule CH_4 or some C-H bearing complex organic molecules. The strong emission feature between 4.4 and 5.0 microns is attributed to emission from CO (see Section 4). Surprisingly enough, no CO_2 emission is detected around 4.3 microns. Strong emission bands in the 3.5–4.2 micron region of the train spectrum remain unexplained at this time.

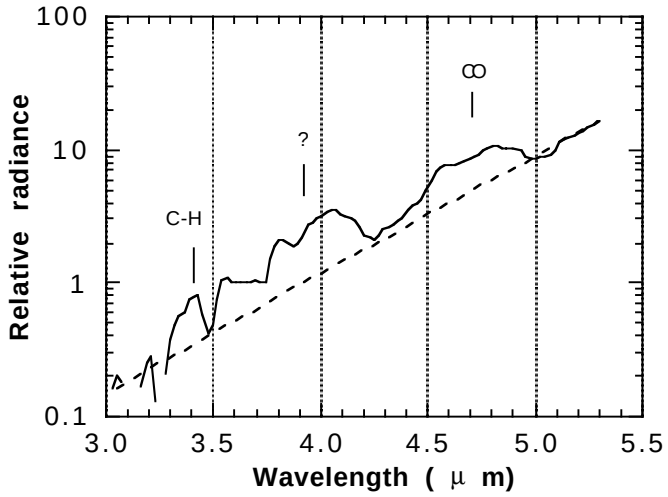

Figure 2b. Semi-log plot of the intensity from the "Y2K" train at 04:02:19 UT reported by MIRIS.

The same data are shown in a semi-log plot to bring out the molecular bands superposed on a continuum rising towards five microns (Figure 2b). Note that the alternative placement of the continuum, with a CO_2 band in absorption, is a less likely choice because it would imply a very high abundance of absorbing molecules and / or solid materials in atmospheric windows from 3.4–4 μm and around 5 μm, for example.

The nature of this continuum is not understood at this time. We are trying to assess the relative likelihood of thermal emission by small solid particles versus a molecular origin such as blended water vapor lines typically found in this part of the spectrum. No optically thick (blackbody) or thin (graybody) thermal emission at T > 1000 K, such as would be seen from hot dust grains, has been detected at this time after the passage of the meteor. Such a hot thermal emission would have resulted in a continuum rising towards shorter wavelength in this regime.

3.2. CVF RESULTS

Ground-based CVF data were obtained on five trains that occurred during the nights of Nov. 17 and 19, 1999 UT. Due to cloud cover on the night of the peak of the shower (Nov. 17/18), no spectra were collected that night. The IR signatures were observed to last at least as long as the visible signatures, in some cases more than 20 minutes. On

the first night at SOR, some of the trains that were seen in the visible had dimmed by the time the platform was pointed in their direction and the IR data were taken even though the visible evidence of the trains on the CCD images was gone. However, IR spectra similar in nature to those shown here were still obtained, suggesting that the IR signatures were longer-lived than the visible emissions.

We present spectra and discuss two trains. The "Puff Daddy" train was caused by a bright Leonid meteor at 10:05 UT on Nov. 19, Az = 34, El = 35. A second train was observed following a bright Leonid at 12:26 UT on Nov. 19, Az = 0, El = 29 to 34 (the trail started at an elevation of 29 degrees, and drifted up to an elevation of 34 degrees, while the instrument tracked the trail as it drifted). Most data pertain to the "Puff Daddy" train, which was about 150–200 km away from the observers at an elevation angle of about 30 degrees.

Three narrow wavelength regimes were studied in coarse spectral steps first. Those wavelength regimes were chosen with the expectation that nitrogen-bearing molecular and CO_2 molecular emissions similar to those seen in auroral displays might be emitting in the meteor train. These narrow wavelength regions are the small pieces shown in Figures 3, 5, and 6. However, because the signal appeared to peak outside the chosen narrow wavelength pieces and we really did not know what to expect, it was decided to map the full wavelength regime (2.5–14.5 microns), which resulted in the full scans shown in Figures 3, 5, and 6. While each wavelength position was integrated and stored, the train gradually decreased in intensity and the spectral shape may also have changed during the scan. It took about 5 minutes to obtain the three narrow regions, and approximately an additional 20 minutes to obtain the three complete spectra. At this point, the train was about 26 minutes old.

3.2.1. The 2.50–4.35 micron wavelength region (wedge 1)

Figure 3 shows the data obtained with the CVF over the short wavelength filter wedge with the emission due to the C-H stretch vibration band prominent at 3.3–3.4 microns. The unidentified emission band at 3.7–4.2 microns is present in the CVF data as well as in the MIRIS data at about the same relative intensity compared to the C-H stretch vibration. Unlike for the MIRIS data, a very rapid increase coinciding with an onset of the CO emission band occurs above 4.0 microns. The data do not appear to have saturated above 4.4 microns and the rapid increase should represent the spectral band shape.

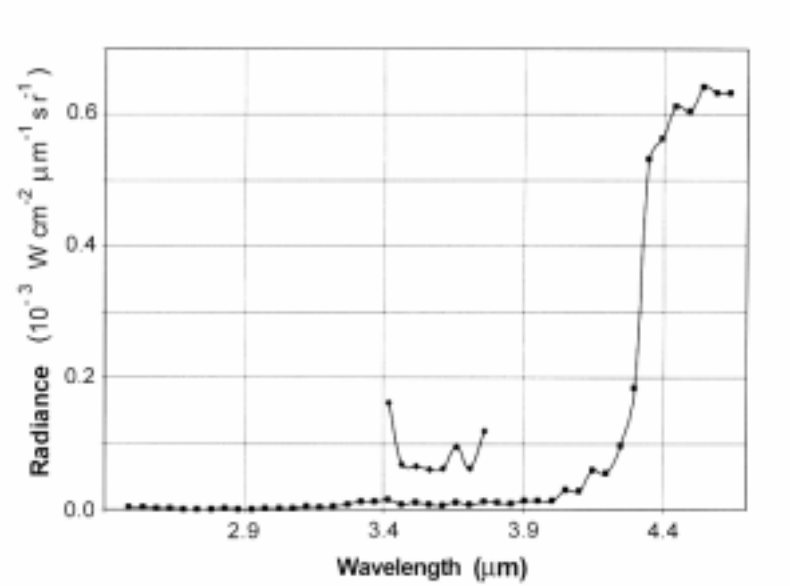

Figure 3. CVF spectra of the train of the meteor that occurred shortly before 10:06 UT, Nov. 19, 1999. The measurements were started at 10:06 UT (short spectrum) and at 10:11 UT (full scan). The effect of the decreasing train intensity between the acquisition of the narrow spectral piece and the full coverage can be seen.

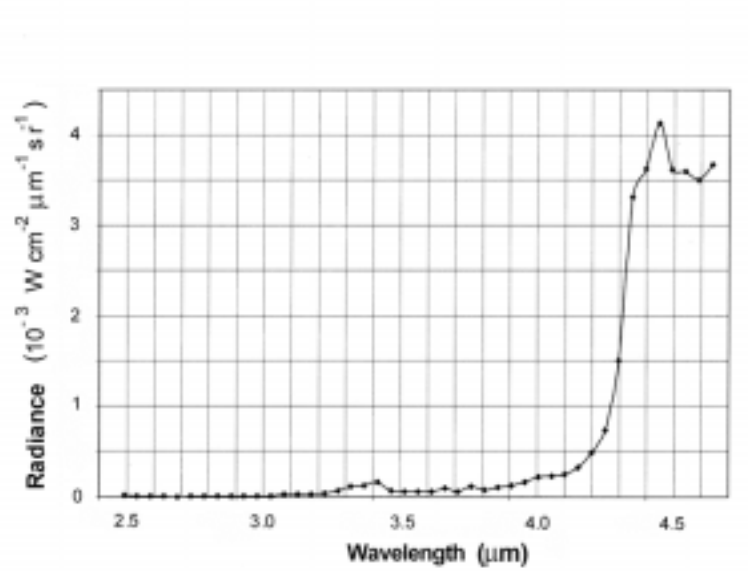

Figure 4. Short wavelength wedge CVF scan of the train of a second meteor at 12:26 UT. These data were taken from 12:27 to 12:32 UT Nov. 19, 1999. Compare to Figure 3.

Given the manner in which the data were taken and processed, that is, by subtracting the spectra obtained while observing the sky at the same elevation as the train but at a different azimuth, one might question the validity of the spectral shapes seen here. The sky signal might not have been constant over the time between meteor data acquisition and sky acquisition, or the elevation angle might not have been accurately set or maintained, or the sky signal shape or amplitude might have been dependent on azimuth. In fact, the shape and amplitude of the sky spectrum repeated well over the entire night for the same elevation angles. However, if spectra of two different meteor trains were to exhibit the same or similar spectral structures while the sky spectra over the night showed differences only at a much smaller signal level, it would lend credence to the data acquisition and processing methods. Thus, for comparison, the spectrum obtained on another meteor in this wavelength region of the spectrum is shown in Figure 4. The spectra of Figures 3 and 4 are very similar. In fact, similarly shaped spectra were obtained on three other Leonid meteor trains during this campaign.

3.2.2. The 4.3–7.8 micron wavelength range (wedge 2)

The detection of the CO_2 band with the CVF occurs only during the first quick scan of one of the three wavelength regions (Figure 5). The band is detected between 4 and 5 microns. In the subsequent full-range scan, the CO_2 emission has decayed considerably.

In the full range spectrum, strong emission attributed to "warm" H_2O is observed. In this context, warm means higher than the typical 200–300 K temperature of water vapor in the lower atmosphere. The CO band emission is not detected, possibly masked by variations in the emission from the ever changing appearance of the train. For the same reason, variations on the gradual rise may also not be spectral features.

The strong rise in the signal above 5 microns was unexpected, considering the normally high opacity of water vapor in the air along the line of sight from the ground to the meteor train. Consequently, the CVF was operated in high gain mode over the 5-8 micron region of the spectrum when observing the trains as well as the (cold) sky. In this mode, the unexpectedly high train signal drove the amplifier into saturation at wavelengths from 6.7 to 7.8 microns.

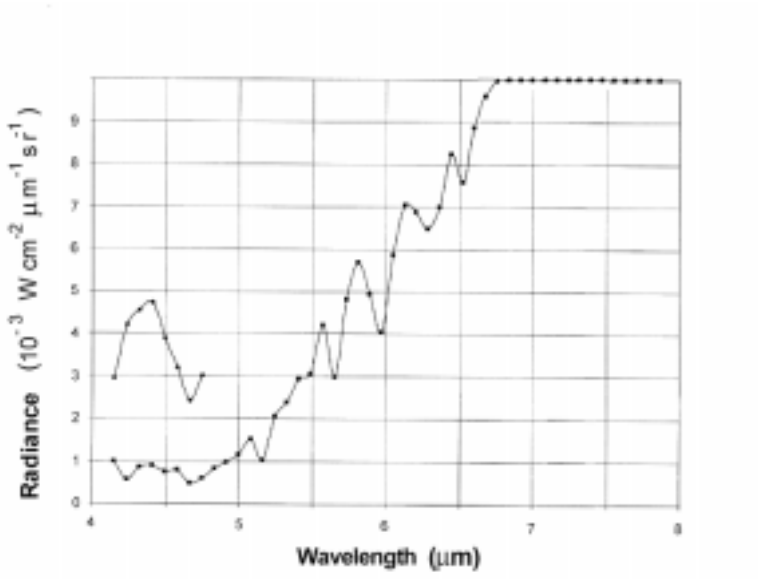

Figure 5. CVF spectrum of the train of meteor 10:05 UT Nov. 19, 1999, taken at 10:16 UT, with a strong H_2O emission peak. Inset shows the earlier narrow scan at time 10:07 UT, with strong CO_2 emission at 4.3 microns (same units as Figure 4).

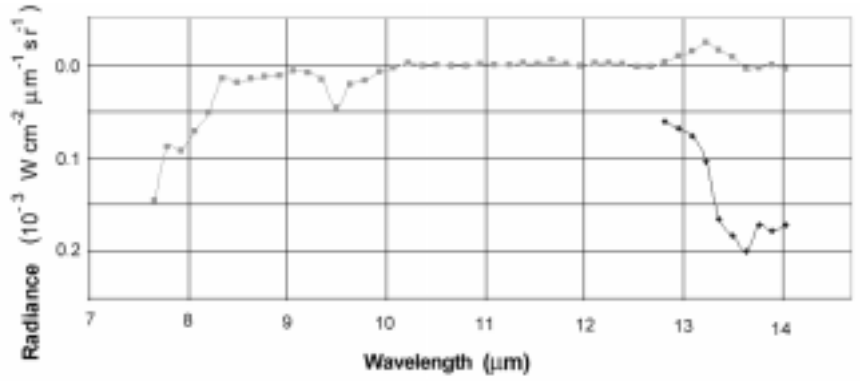

Figure 6. CVF spectrum from 7.5 to 14.5 microns of the same train observed to obtain the data shown in Figures 3 and 5. The data acquisition consisted of taking the short pieces in all three figures first, followed by the acquisition of the entire 2.5 to 14 micron spectrum. The strong absorption seen near 13 – 14.5 microns is unexplained, as is the dip from 7.7 to 8.3 microns (same units as Figures 4 and 5).

3.2.2. The 8–14 micron wavelength range (wedge 3)

The data acquisition in wedge 2 is stopped after 7.8 microns, the gain changed from high to low, the filter wheel advanced to the third filter wedge, and the user prompted for an input that it is OK to continue the data acquisition. This procedure takes more than enough time for the saturation effect of the instrument to go away in the next (8–14 micron) range, and the change to low gain also speeds up the electrical recovery from saturation.

Figure 6 shows the CVF data of the long wavelength regime from the same train that was observed to obtain the data shown in Figures 3 and 5. The scale is significantly expanded. This spectrum exhibits a puzzling downturn at wavelengths greater than 13 microns, which was more prominent in the earlier narrow spectral scan than in the later full scan. This occurs in the part of the spectrum dominated by the edge of the 16-micron atmospheric CO_2 band. The decreased emission longward of 13 microns was seen in all three trains observed with the CVF at these wavelengths.

The full scan taken later in time also exhibits an unexplained dip in the 7.7 to 8.3 micron region. (The small negative signal from ~8.3 to 10 microns is consistent with the uncertainty in the sky subtraction process, and the 9.6 micron dip may well be due to the known azimuth-dependence of ozone emission from the sky.) There is not enough additional data around 8 microns on other trains to address the reality of this dip in the train spectrum, and it seems inconsistent with the large excess observed with wedge 2 (Figure 5) just a short time before. We believe the multiple train observations of the enhanced 5–8 micron emission and the 13–14 micron dips are evidence for those features being real, but we do not have enough data for the 7.7–8.3 micron region to make a similar claim. Additional data will have to be acquired on more trains to address this issue.

4. Discussion

The emissions here reported do not originate from airglow-type chemistry that was proposed as an explanation for the optical luminosity features observed (Kelley *et al.,* 2000; Jenniskens *et al.,* 2000b). The mid-IR spectral features are assigned to enhanced emissions of CO, CO_2, CH_4 and H_2O, which may originate from heated trace air compounds or

materials created in the wake of the meteor. None of the molecules detected here has been observed in the visible range. As such, the mid-IR observations offer a whole new perspective on the physical properties of meteor trains.

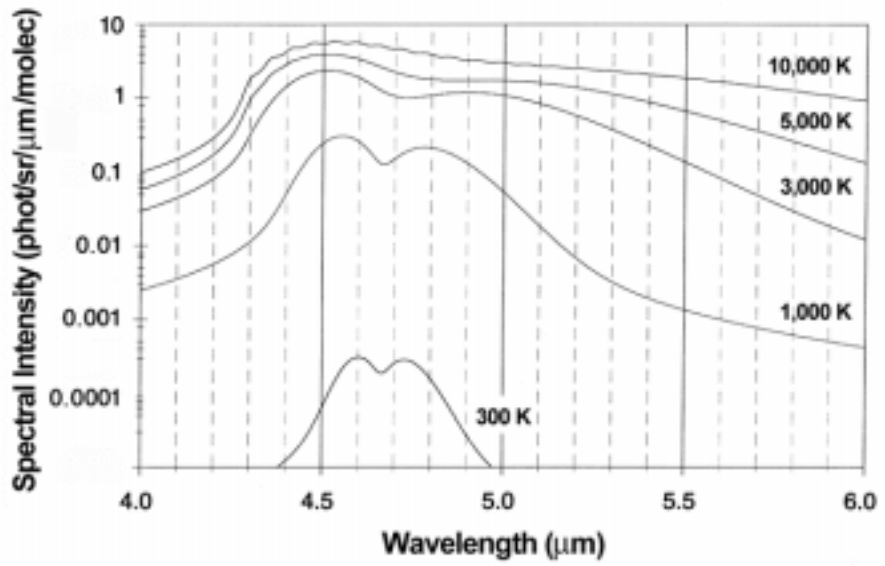

Figure 7. Model calculations for hot, optically-thin CO molecules. These spectra go from cool on the bottom to hot on the top. They have been smoothed to a resolving power of 100 to better compare the shapes with the train data.

4.1. CO

The shape of thermal emission bands can be used to determine the excitation temperature of the responsible molecules. Figure 7 shows calculations for the CO molecule that is believed to be responsible for the band between 4.4 and 5.0 microns. The shape is significantly broader at the high temperatures of T ~ 5,000 K and T ~10,000 K that are reported for the hot and warm visible emissions from meteors. The train emission is more typical for a gas at T ~ 300 K, which is consistent with the observation by Borovicka and Jenniskens (2000) that the Y2K train temperature decreased from ~4,500 K to ~1,200 K in a mere two seconds. It is also consistent with the results from Chu *et al.* (2000), which determined the temperature of sodium emission from persistent trains using LIDAR measurements of the Doppler broadening of the

resonant scattering profile. Chu *et al.* (2000) found elevated gas temperatures of about 230 K at 92.2 km altitude and 260 K at 92.35 km altitude, which is ~50 K above the background ambient Na temperature of 210 K, observed 2.9 minutes after the meteor's first appearance. This time lapse is similar to that present for our observations.

4.2. CO_2

Warm CO_2 is observed by the CVF instrument in the persistent train spectra immediately after train formation. The initial scan of Figure 5 about 2 minutes after the meteor shows the emission at the expected position. It is not observed in the MIRIS data 1m52s after train formation and has declined to background levels in a subsequent CVF scan taken 9 minutes later. A rapid decline of the CO_2 emission is implied, perhaps responsible for the lack of CO_2 emission in the MIRIS data.

4.3. C-H

The C-H stretch vibration is observed in all MIRIS and CVF data. The band is not well resolved. It has a gradual rise above 3.27 microns, with possibly two maxima at 3.35 and 3.42 microns and a sharp downturn above 3.46 microns (see first scan Figure 3).

The 3.4 microns feature in room temperature cometary dust typically has a similar asymmetric peak with a broad maximum at 3.38 microns and a steeper downturn at the long wavelength edge (e.g. Encrenaz and Knacke, 1991), and is characteristic of complex organic matter rich in CH_2 and CH_3 groups. Additional modeling will be required for the detailed interpretation of the origin of the emission structure, but the Occam's Razor assignment would be to the simple, easy to form, prevalent molecule CH_4. However, we can't rule out more complex molecules or even organic solids at this time.

4.4. H_2O

As we consider wavelengths long-ward of 5 microns in Figure 5 (and the implication of the trend in the MIRIS data in Figure 2a), we see a gradual rise towards 6.7 microns. It is likely that the gradual rise is followed by a decline of emission at wavelengths above 6.7 microns as suggested by subsequent observations in the 8–14 micron range.

It is not certain that the rise itself must be due to warm water vapor band emission centered at 6.24 microns, or whether there may be thermal dust continuum emission analogous to that seen in cometary spectra. However, the absence of strong continuum dust emission in the 8–13 micron region (wedge 3, Figure 6) argues against a broad thermal dust continuum with or without silicate emission, and is consistent with the rapid decline expected in warm water vapor emission beyond 7 microns.

One difficulty with the warm water vapor interpretation is that the warm gas must have a temperature above 200–300 K relatively long after the meteor, to avoid being completely absorbed by warm lower atmospheric water vapor between the ground-based observation station and the meteor train.

4.5. OTHER FEATURES

Given the detection of CO_2 band emission at 4.2 microns (Figure 5, narrow scan), it was expected that strong CO_2 band emission would arise above 13 microns in the first narrow scan of Figure 6. However, it is unknown how a lack of emission in the long wavelength 16 micron CO_2 band can be explained in relation to the distant train. The constancy of the atmospheric emission at these wavelengths over the course of the night implies much less variation over the relatively short time between the observations of the train and of the sky (at the same elevation angle, but slightly different azimuth, a few minutes later) than the difference between the train and the sky. As long as the atmospheric emission is constant, this strongly suggests that the observed dip is a real phenomenon, and not an artifact of the sky subtraction process. The fact that the dip was seen in all the train spectra at these wavelengths (at least 3) is viewed as evidence for some real effect other than inaccurate sky subtraction. As we expected most of the observed CO_2 emission to originate close to the sensor along the line of sight from the ground to the train, and not to originate in the train itself, additional modeling of the amount of emission and absorption as a function of position along the line of sight will be undertaken in an effort to understand the data.

4.6. SYNTHESIS

Given our understanding of meteor grains based on spectroscopy of parent cometary dust, it is unlikely that the molecules that we believe are responsible for the emission reported here existed in molecular form in

the meteor. It is more likely that the observed emissions are due to heating of ambient air molecules (atmospheric molecules that existed prior to the passage of the meteor), all of which are present (albeit at very low densities) at altitudes of ~85 km in the quiet atmosphere before passage of the meteor.

It is also possible that the interaction of the meteor with the Earth's atmosphere at 72 km/sec caused material to ablate and vaporize, forming a hot atomic gas. The laboratory analyses of chondritic interplanetary dust particles that include dust of cometary origin show the presence of silicate minerals and organic matter (Rietmeijer and Nuth, 2000). Thus, the dust grains that made up the meteor could be sources for the atoms in the gas species that we observed. The evolved atomic gas from the ablation process cooled and formed the excited molecules whose IR emissions are reported here.

Future work will use the Modtran software package to ascertain whether the water vapor could be ambient atmospheric molecules excited by the passage of this meteor, or whether the very dry conditions at the meteor altitude of ~85 km combined with the strength of the emissions suggests or requires that the hydrogen and oxygen came from organic and mineral components in the meteor, respectively. Note that this does not require that the meteor body contained water (such as in layer silicate minerals) or water ice. Vaporization of the meteor body may have broken down organic and inorganic materials into atomic species, thus freeing the hydrogen and oxygen necessary to produce the water seen in emission in these data.

Further evidence may also be present in the totality of the current set of data. The MIRIS data from multiple pointings at the train (as opposed to the single spectrum shown here), and over a seven minute time span, will provide a series of spectra that follows the CO and C-H emission evolution over time. These data are expected to provide detailed information about the temperature evolution in the train and the physical conditions in the meteor path for the long time scales at which organic chemistry and metal atom chemistry between meteor material and ambient air molecules occurs.

5. Summary

IR spectroscopy of persistent Leonid meteor trains shows prominent molecular band emissions at 3.4, 4.0, 4.3, 4.7, and 6–7 microns. The

commonality of the spectra obtained from two platforms, one on the ground and one airborne, and with two dramatically different sensors, lends strong credence to the validity of the spectral structure seen emanating from these long-lived trains. Not all features have been identified with certainty. Obvious candidates are CH_4, CO, CO_2, and H_2O. No optically thick or thin thermal emission at > 1000 K has been seen to date, but continuum emission from cold ~ 300 K sources may be present. However, we have seen no evidence for expected emission in the wavelength region of the Si-O stretch vibration at 10 micron. The exact emission/excitation mechanisms for the long-lived (in some cases more than 20 minutes) IR signatures are still not understood. Future work will include modeling of the passage of the meteor through the atmosphere to investigate the heating and cooling of meteoric and atmospheric materials, and to model the molecular emissions at the various wavelengths to discriminate between atmospheric and meteoroid sources for the atoms.

Acknowledgments

We are grateful to the staff and crew of the FISTA and SOR, without whose strong support this work could not have been accomplished. This research is supported at The Aerospace Corporation by the Internal Research and Development program. The Leonid MAC was supported by NASA's Exobiology, Planetary Astronomy and Suborbital MITM programs, as well as by NASA's Advanced Missions and Technologies program for Astrobiology and NASA Ames Research Center. We thank Joe Kristl and his group at Space Dynamics Laboratory, Utah State University, for their assistance in the FISTA installation and operation, and for the loan of an eyeball mount and ZnSe window for use with MIRIS. Paul Zittel, The Aerospace Corporation, is acknowledged for providing the molecular emission spectra of CO. We thank referee Diane Wooden, whoes comments helped improve the paper. *Editorial handling*: Frans Rietmeijer.

References

Borovicka, J. and Jenniskens, P.: 2000, *Earth Moon and Planets* **82–83**, 399–428.
Boyd, I.D.: 2000, *Earth Moon and Planets* **82–83**, 93–108.

Chu, X., Liu, A.Z., Papen, G., Gardner, C.S., Kelley, M., Drummond, J., and Fugate, R.: 2000, *Geophys. Res. Lett*. **27**, 1815–1818.

Encrenaz, T. and Knacke, R.: 1991 in R.L. Newburn, Jr., M. Neugebauer, J. Rahe (eds.), *Comets in the Post-Halley Era*, Vol. 1, 107–137.

Hanner, M. S., Lynch, D. K., and Russell, R. W.: 1994, *Astrophys. J.*, **425**, 274–285.

Jenniskens, P. and Butow, S.J.: 1999, *Meteoritics Planet. Sci.* **34**, 933–943.

Jenniskens, P. and Rairden, R.: 2000, *Earth, Moon and Planets* **82–83**, 457–470.

Jenniskens, P., Butow, S.J., and Fonda, M.: 2000a, *Earth Moon and Planets* **82–83**, 1–26.

Jenniskens, P., Nugent, D., and Plane, J.M.C.: 2000b, *Earth, Moon and Planets* **82–83**, 471–488.

Kelley, M.C., Gardner, C., Drummond, J., Armstrong, T., Liu, A., Chu, X., Papen, G., Kruschwitz, C., Loughmiller, P., Grime, B., and Engelman, J.: 2000, *Geophys. Research Letters* **27**, 1811–1814.

Lynch, D.K., Russell, Ray W., and Sitko, M. L.: 2000, *Icarus*, **144**, 187–190

Popova, O.P., Sidneva, S.N., Shuvalov, V.V., and Strelkov, A.S.: 2000, *Earth Moon and Planets* **82–83**, 109–128.

Rossano, G.S., Russell, R.W., Lynch, D.K., Tessensohn, T.K., Warren, D., and Jenniskens, P.: 2000, *Earth Moon and Planets* **82–83**, 81–92.